2023 American Control Conference (ACC)
San Diego, CA, USA. May 31 - June 2, 2023

Simultaneous Motion and Stiffness Control for Soft Pneumatic Manipulators based on a Lagrangian-based Dynamic Model

Yu Mei[1], Preston Fairchild[1], Vaibhav Srivastava[1], Changyong Cao[2], and Xiaobo Tan[1]

Abstract— **A soft continuum manipulator with tunable stiffness can not only take advantage of high compliance for safe adaptation in unknown environments, but also circumvent the drawbacks of instability and low loading capability. The high nonlinearity of soft manipulators and the strong coupling between actuation and stiffness-tuning make their simultaneous control challenging. In this work, a novel approach to simultaneous control of actuation and stiffness-tuning is proposed for soft pneumatic manipulators. With a piecewise-constant curvature assumption, a Lagrangian-based dynamic model with realistic approximation is used for control design, where the dynamics of the stiffness-tunable mechanism is incorporated. An extended Kalman filter (EKF) is proposed to estimate unmeasurable states including the stiffness and the velocity. A nonlinear model predictive control (NMPC) framework is developed first in the configuration space, and then extended to the task space, for simultaneous motion and stiffness control under inflation and vacuum pressure constraints. Simulation results are presented to support the efficacy of the proposed approach.**

I. INTRODUCTION

Compared to conventional rigid robots, soft robots offer greater flexibility and safety, making them more suitable for interactions with delicate objects and humans, for example, in grasping fruits, providing assistance in rehabilitation, and performing minimally invasive surgeries [1]–[3]. The intrinsic compliance of soft robots, on the other hand, poses a formidable challenge when exerting force and maintaining shapes. It is critical to design soft continuum manipulators and associated control schemes that leverage the dexterity and adaptiveness of soft robots as well as inherit the strength and stability of rigid robots.

There have been a variety of methodologies proposed for motion control of soft continuum manipulators, including model-free and model-based methods [4]. Model-free methods circumvent the uncertainties and complexities of soft robot dynamics and provide motion control directly, but they require extensive learning and training on existing prototypes [5], [6]. Model-based methods attract significant attention since they are typically more easily adaptable to different scenarios, examples of which include the principle of virtual power [7] and the Cosserat theory [8]. However, control strategies based on these theories are typically limited to handling only quasi-static problems and require intensive computation. A Piecewise Constant Curvature (PCC) assumption is commonly adopted to approximate the configuration of continuum manipulators and ease their modeling and control design. There is an emerging trend towards control-oriented dynamic models with the PCC assumption. An Augmented Rigid Body Model was recently proposed in [9], which utilizes multiple rigid links to approximate the real kinematics and dynamics of the soft continuum robots. Based on this model, a number of control schemes including adaptive control and model predictive control (MPC) [10], [11], have been designed. However, this approach tends to suffer from requiring high computation of abundant rigid states. To address this issue, a Lagrangian-based dynamic model with realistic approximation has gained significant attention [12]. It inherits the approximation idea and friendly extensibility of the Augmented Rigid Body Model and is much faster to implement. Nevertheless, all aforementioned works have not taken stiffness control into consideration, which is critical in practical applications of soft robots.

In the last few years, researchers have been developing various soft robots with tunable stiffness [3], [13], [14]. However, the majority of them model the stiffness as discrete states based on experimental calibration and do not control the stiffness continuously. Continuous stiffness control provides advantages such as precise motion control with different contact forces, eliminating unwanted dynamics, and achieving movements from releasing stored energy. There are a few works modeling continuously tunable stiffness based on energy methods [15], [16], but they are focused on the planar case and do not address accurate dynamic motion control. Interestingly, fully exploiting the potential of motion dynamics and tunable stiffness in rigid manipulators, as in variable stiffness actuators (VSA), is a topic of significant interest in the scientific community [17]. To our best knowledge, this contribution to simultaneous motion and stiffness control has not yet been made for soft continuum manipulators. The most closely related work may be a sliding model controller and a model predictive control for simultaneous position and stiffness control of an inflatable soft robot [18]. However, the movement of the robot is restricted to the 2D plane as it is generated by two antagonistic air bladders. Additionally, the work is limited by the fact that it uses a linear dynamic model of a single degree of freedom (DoF). Since soft manipulators with multiple segments in three dimensions have high nonlinearity, this work cannot be readily extended to soft manipulators in general.

*This research was supported in part by National Science Foundation awards ECCS 2024649 and CMMI 1940950.

[1]Yu Mei, Preston Fairchild, Vaibhav Srivastava and Xiaobo Tan are with the Department of Electrical and Computer Engineering, Michigan State University, East Lansing, MI 48823, USA. Email: meiyu1@msu.edu, fairch42@msu.edu, vaibhav@egr.msu.edu, xbtan@egr.msu.edu

[2]Changyong Cao is with Department of Mechanical & Aerospace Engineering, Case Western Reserve University, Cleveland, OH 44106 USA. Email: ccao@case.edu

In this paper, we present a model considering controllable stiffness and a novel nonlinear MPC (NMPC) framework for simultaneous motion and stiffness control of a soft continuum manipulator. In Section II, a model for tunable stiffness is incorporated into an accurate dynamic model with realistic approximation. In Section III, we describe the NMPC framework for simultaneously tracking desired motion trajectory in the configuration space and the desired stiffness trajectory, followed by an extension to the motion control in the task space. Simulation results are demonstrated in Section IV, followed by concluding remarks in Section V.

II. MATHEMATICAL MODELING

To design the controller for the soft manipulator system, we first describe the model to be used. In this work, three assumptions have been imposed on the soft manipulator:
A1: The material distributed along the length of manipulator is homogeneous, which facilitates the calculation of the center of mass.
A2: The length of the centerline of the manipulator is constant irrespective of its bending [9].
A3: Fiber-reinforced structures reduce the effects of radial ballooning, so the manipulator has no radial expansion [19], meaning that the cross-section retains its structure when bending, and the second moment of inertia remains constant.

A. Kinematic and Dynamic Models

The kinematic model of the soft continuum manipulator is based on the PCC approach, which has been widely used. This approach describes each segment of the soft arm as a constant curvature, with the curvature varing between different segments. Let the entire arm shown in Fig. 1(a) have n segments. There is a coordinate frame $\{S_i\}$ attached to the tip of the i-th segment, and a base frame $\{S_0\}$ fixed to the base. The homogeneous transformation matrix T_j^i expresses the position and orientation of $\{S_j\}$ with respect to $\{S_i\}$. Additionally, for each segment, arc parameters $(\phi_i, \theta_i)^T$ are defined as generalized coordinates q_i, where ϕ is the angle between the x-z plane and arc plane, and θ is the bending angle as depicted in Fig. 1(b). $q \in \mathbb{R}^{2n}$ describes the configuration of the entire arm and it collects all coordinates in the form $(q_1, q_2 \cdots q_n)^T$.

The homogeneous transformation matrix mapping from $\{S_{i-1}\}$ to $\{S_i\}$ can be written as [20]:

$$T_i^{i-1}(\phi_i,\theta_i) = \begin{bmatrix} C_{\phi_i}^2(C_{\theta_i}-1)+1 & S_{\phi_i}C_{\phi_i}(C_{\theta_i}-1) & C_{\phi_i}S_{\theta_i} & \frac{L_i}{\theta_i}C_{\phi_i}(1-C_{\theta_i}) \\ S_{\phi_i}C_{\phi_i}(C_{\theta_i}-1) & C_{\phi_i}^2(1-C_{\theta_i})+C_{\theta_i} & S_{\phi_i}C_{\theta_i} & \frac{L_i}{\theta_i}S_{\phi_i}(1-C_{\theta_i}) \\ -C_{\phi_i}S_{\theta_i} & -S_{\phi_i}S_{\theta_i} & C_{\theta_i} & S_{\theta_i} \\ 0 & 0 & 0 & 1 \end{bmatrix}, \tag{1}$$

where L_i is the length of i-th segment and C_{ϕ_i}, S_{ϕ_i}, C_{θ_i}, and S_{θ_i} are the abbreviation of $\cos(\phi_i)$, $\sin(\phi_i)$, $\cos(\theta_i)$, and $\sin(\theta_i)$, respectively.

As mentioned in [21], it is reasonable to assume that the mass of each section can be approximated by lumping it into a single mass point. Instead of taking the over-simplified assumption that the mass point is concentrated at the segment's tip as in [21], the mass point is considered to be located at the centroid of each segment, which is on the line connecting the center of curvature and the middle of the arc, as shown in Fig. 1(b). As indicted in [12], this representation of center of mass (CoM) is more realistic. The position of the CoM in the i-th segment in the inertial frame $p^0_{i\text{-CoM}}$ can be computed as:

$$\begin{bmatrix} p^0_{i\text{-CoM}} \\ 1 \end{bmatrix} = T_1^0(\phi_1,\theta_1)\cdot T_2^1(\phi_2,\theta_2)\cdots T_i^{i-1}(\phi_i,\theta_i)\cdot \begin{bmatrix} p^i_{i\text{-CoM}} \\ 1 \end{bmatrix}, \tag{2}$$

where T_i^{i-1} is formulated in Eq. (1), and $p^i_{i\text{-CoM}}$ is the i-th CoM in its local frame, which can be computed as:

$$p^i_{i\text{-CoM}} = R_z(\phi_i)R_y(\frac{\theta_i}{2}) \begin{bmatrix} \frac{L_i}{\theta_i}\cos\frac{\theta_i}{2} - \eta_i \\ 0 \\ \frac{L_i}{\theta_i}\sin\frac{\theta_i}{2} \end{bmatrix}, \tag{3}$$

where $R_z(\phi_i)$, $R_y(\frac{\theta_i}{2}) \in SO(3)$ are the representive rotation matrices and η_i is the distance between the center of the arm and its CoM, and is given by [9]:

$$\eta_i = \frac{2L_i \sin\frac{\theta_i}{2}}{\theta_i^2}. \tag{4}$$

The dynamic equation of the soft manipulator can be derived by the Euler-Lagrange approach. The classical Euler-Lagrange equation is $\frac{d}{dt}\frac{\partial L}{\partial \dot{q}} - \frac{\partial L}{\partial q} = f$, where L is the Lagrangian derived by subtracting the total potential energy from the total kinetic energy, and f is the generalized force associated with q. In this model, the potential energy of the i-th segment can be computed by the position of its CoM, and the individual kinematic energy can also be computed given the velocity of the CoM in the inertial frame. With this approach, one can derive the dynamic equation $M(q)\ddot{q} + V(q,\dot{q}) + G(q) = \tau$, where $M(q) \in \mathbb{R}^{2n\times 2n}$, $V(q,\dot{q}) \in \mathbb{R}^{2n}$, $G(q) \in \mathbb{R}^{2n}$, and $\tau \in \mathbb{R}^{2n}$ are the inertia matrix, the centrifugal and Coriolis term, the gravitational term, and the generalized torque, respectively. As an attempt to mimic the characteristics of the real soft manipulator, the springs and

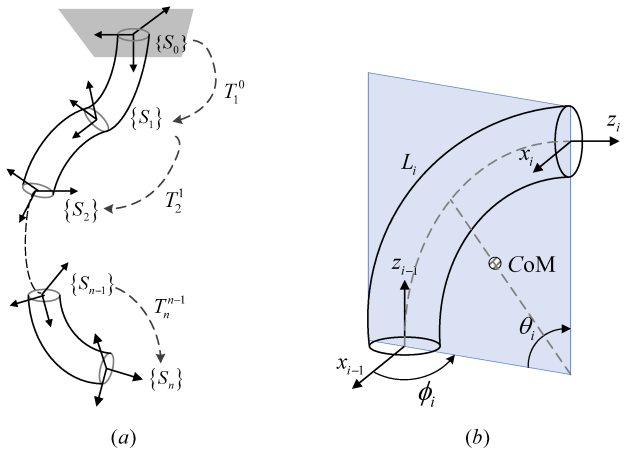

Fig. 1. Kinematic representation of a soft continuum arm under the PCC assumption. (a) Reference frames $\{S\}$ of the entire arm and the transformation matrix $\{T\}$ between neighbour segments. (b) The illustration of the parameters of PCC representation for i-th segment, where CoM is the center of mass of the segment.

dampers are assumed to be distributed continuously along the arm's cross-section. The dynamic model is defined as follows by adding the stiffness and damping items into the previous general dynamic equation:

$$M(q)\ddot{q} + V(q,\dot{q}) + D(q)\dot{q} + G(q) + Kq = A(q)\tau_A, \quad (5)$$

where $D(q) \in \mathbb{R}^{2n\times 2n}$ is the damping matrix, $K(q) \in \mathbb{R}^{2n\times 2n}$ is the stiffness matrix, and $A(q) \in \mathbb{R}^{2n\times 2n}$ is the mapping matrix converting $\tau_A \in \mathbb{R}^{2n}$, the equivalent torque around x and y axes, to generalized torque τ. These matrices are all defined in [9].

B. Pneumatic Drive and Actuation Dynamics

For the sake of conciseness, the i-th segment is utilized for analysis. In Eq. (5), for control purposes, it is easier to use an orthogonal and bi-directional "pseudo-torque" $\tau_{A,i} = [\tau_{x,i}, \tau_{y,i}]^T$ for actuation of each segment. For an actual omnidirectional bending manipulator, three uniformly distributed air inflation chambers controlled independently by positive pressures are typically used, as shown in Fig. 2. Therefore, it is necessary to translate the actual actuation pressure into their pseudo-torque, and the pseudo-torque of the i-th segment can be formulated in the following form:

$$\tau_{A,i} = T_i \cdot W_i \cdot P_i, \quad (6)$$

where P_i is the vector indicating the actual pressure of the three chambers, W_i is the mapping matrix converting actual pressure to its equivalent moment applied on the manipulator, and T_i is the mapping matrix combining the three individual moments to pseudo-torque around the x-y axis. These matrices are defined by:

$$\begin{aligned} P_i &= \begin{bmatrix} P_{i,1} & P_{i,2} & P_{i,3} \end{bmatrix}^T, \\ W_i &= \begin{bmatrix} w & 0 & 0 \\ 0 & w & 0 \\ 0 & 0 & w \end{bmatrix}, \\ T_i &= \begin{bmatrix} 1 & -\frac{1}{2} & -\frac{1}{2} \\ 0 & \frac{\sqrt{3}}{2} & -\frac{\sqrt{3}}{2} \end{bmatrix}, \end{aligned} \quad (7)$$

where $P_{i,1}, P_{i,2}, P_{i,3}$ are the actual pressures of the three chambers and w is the actuation parameter.

The pressures cannot be directly controlled due to pneumatic actuation dynamics, and instead they result from the closed-loop tracking of some desired references (by, for example, a PID controller). The dynamics of the underlying pressure can be captured in a first-order model [22]:

$$\begin{aligned} \dot{P}_{i,j} &= a_0 P_{i,j} + a_1 P_{i,j,\text{des}}, \\ & i = 1,2,\ldots,n, \quad j = 1,2,3, \end{aligned} \quad (8)$$

where $P_{i,j}$ is the pressure of the j-th air chamber in the i-th segment, $P_{i,j,\text{des}}$ is the desired pressure of the corresponding chamber, and a_0 and a_1 are constant parameters, which could be obtained by fitting a step response.

C. Dynamic Model for Tunable Stiffness

In order to realize the stiffness-tunable function, a variety of approaches have been developed, such as jamming actuation [23] and material-based methods [24]. Although our control approach is not limited to specific stiffness-tunable mechanisms, a particle jamming mechanism is taken as an example here to derive the dynamic model of stiffness tuning due to the fact that it is simple, fast, and can be controlled continuously [25]. The particles in an enclosed space can move freely without external force but jam against each other firmly under vacuum pressure [26]. As shown in Fig. 2, suppose that the core section of a soft manipulator is replaced by a stiffness-tunable core with a particle jamming mechanism. Consequently, the stiffness matrix K_i could be divided into two parts:

$$\begin{aligned} K_i &= K_{i,\text{outer}} + \left(\frac{r}{R}\right)^2 K_{i,\text{core}} \\ &= \left[1 - \left(\frac{r}{R}\right)^2\right] K_i^0 + \left(\frac{r}{R}\right)^2 K_{i,\text{core}}, \end{aligned} \quad (9)$$

where K_i is the stiffness matrix of the i-th segment, which composes the full stiffness matrix $K(q)$ from Eq. (5) by block diagonal concatenations. $K_{i,\text{outer}}$ is the stiffness matrix of the outer manipulator body, $K_{i,\text{core}}$ is the tunable stiffness matrix of the inner core, $K_i^0 = \begin{bmatrix} 0 & 0 \\ 0 & k_i^0 \end{bmatrix}$ is the constant stiffness matrix of soft manipulator before removing the core, and R and r are the radii of the outer manipulator body and inner core respectively. The full derivation is not presented, but it can be derived easily based on the derivation that the stiffness is directly proportional to the material's Young's modulus [27].

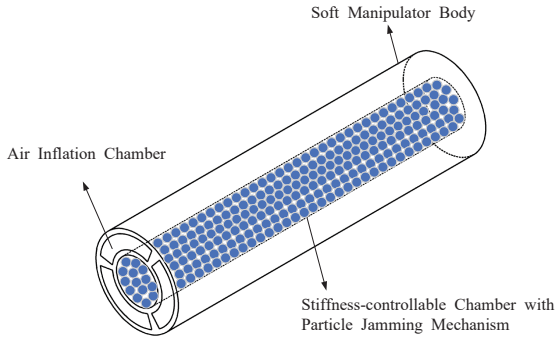

Fig. 2. Illustration of a soft manipulator with stiffness-tunable core.

The stiffness of the particle jamming mechanism is determined by the differential pressure between the pressures in the air chambers and the particle chamber. An actuator based on differential-drive particle jamming has the advantage of achieving simultaneous deformation and stiffness variation [15]. As reported by [26], the stiffness of passive particle jamming is proportional to the actuator's air pressure, so a reasonable assumption is made that the stiffness of the inner core varies linearly with differential pressure. Under

this assumption, the stiffness matrix of the inner core $K_{i,\text{core}}$ is defined as:

$$K_{i,\text{core}} = \begin{bmatrix} 0 & 0 \\ 0 & k_{i,\text{core}} \end{bmatrix},$$
$$\text{where } k_{i,\text{core}} = \alpha \left[\frac{1}{3}(P_{i,1} + P_{i,2} + P_{i,3}) + P_{i,\text{core}} \right], \quad (10)$$

where α is the constant coefficient mapping the differential pressure to the stiffness of the core and $P_{i,\text{core}}$ is the absolute value of the vacuum pressure in the core chamber. An important note is that $P_{i,\text{core}}$ is computed by subtracting vacuum pressure from the atmosphere pressure (0 kPa), which means $P_{i,\text{core}}$ is always positive. Similarly to Eq. (8), the pneumatic actuation dynamics in the particle chamber can be written as:

$$\dot{P}_{i,\text{core}} = b_0 P_{i,\text{core}} + b_1 P_{i,\text{core,des}}, \quad (11)$$

where $P_{i,\text{core,des}}$ is desired pressure of particle chamber in the i-th segment's core, and b_0 and b_1 are constant parameters.

D. Full Model

The models of the subsystems in Section II A-C can be combined to obtain the full dynamics of the soft continuum manipulator. The stiffness of the inner core in Eq. (10) depends on the pressures of all four chambers, while the pressure in the central particle chamber does not actuate the bending motion of the manipulator, as expressed in Eq. (6). In order to make the following formulation more uniform and brief, the pressure of the particle chamber $P_{i,\text{core}}$ is merged into the pressure vector P_i from Eq. (7) and the mapping matrix W_i is augmented as follows:

$$P_i = \begin{bmatrix} P_{i,1} & P_{i,2} & P_{i,3} & P_{i,\text{core}} \end{bmatrix}^T,$$
$$W_i = \begin{bmatrix} w & 0 & 0 & 0 \\ 0 & w & 0 & 0 \\ 0 & 0 & w & 0 \end{bmatrix}. \quad (12)$$

With the substitution of (6) and (9) into (5), the full dynamic equation of the manipulator could be rewritten as:

$$M(q)\ddot{q} + V(q,\dot{q}) + D(q)\dot{q} + G(q) + \left[1 - \left(\frac{r}{R}\right)^2\right] K^0 q$$
$$= A(q) \cdot T \cdot W \cdot P - \left(\frac{r}{R}\right)^2 K_{\text{core}}(P) q, \quad (13)$$

where $T \in \mathbb{R}^{2n \times 3n}$ and $W \in \mathbb{R}^{3n \times 4n}$ are the direct matrix sum of T_i in (7) and W_i in (12), respectively, $P \in \mathbb{R}^{4n}$ is the one-dimensional column vector concatenated of P_i in (12), $K^0 \in \mathbb{R}^{2n \times 2n}$ is the block diagonal concatenation of K_i^0, and $K_{\text{core}}(P)$ is the block diagonal concatenation of $K_{i,\text{core}}$ in (10).

Based on Eq. (9) and (10), the stiffness of the i-th segment k_i can be written as:

$$k_i = \alpha \left(\tfrac{r}{R}\right)^2 \left[\tfrac{1}{3}(P_{i,1} + P_{i,2} + P_{i,3}) + P_{i,\text{core}}\right] + \left[1 - \left(\tfrac{r}{R}\right)^2\right] k_i^0. \quad (14)$$

III. CONTROL DESIGN

As discussed in the previous section, it is evident that bending motion and stiffness variation have mutual interactions. Thus, it is a challenging task to control the position and stiffness simultaneously in this highly nonlinear Multi-Input Multi-Output (MIMO) system. The control objective of this work is to track the desired position trajectory and desired stiffness trajectory. In this section, an NMPC framework is proposed for the soft continuum manipulator in the configuration space, and is subsequently extended to the task space.

A. State Dynamics

In order to realize stiffness control, the stiffness will be included as a state variable [18]. By taking the derivative of Eq. (14) with respect to time and then plugging Eq. (8) and (11) into it, the differential equation for stiffness is obtained:

$$\dot{k}_i = \alpha \left(\frac{r}{R}\right)^2 [\frac{1}{3} a_0 (P_{i,1} + P_{i,2} + P_{i,3}) + b_0 P_{i,\text{core}}$$
$$+ \frac{1}{3} a_1 (P_{i,1,\text{des}} + P_{1,2,\text{des}} + P_{i,3,\text{des}}) + b_1 P_{i,\text{core,des}}]. \quad (15)$$

In this work, the PCC coordinates, the velocity of said coordinates, the joint stiffness, and pressures in every chamber are defined as system states $\mathbf{x} \in \mathbb{R}^{9n}$, and the desired pressures or pressure set points sent to the underlying controller are defined as the system input $\mathbf{u} \in \mathbb{R}^{4n}$:

$$\mathbf{x} = \begin{bmatrix} q & \dot{q} & K_J & P \end{bmatrix}^T,$$
$$\mathbf{u} = P_{\text{des}}$$
$$= \begin{bmatrix} P_{1,\text{des}} & \cdots & P_{i,\text{des}} & \cdots & P_{n,\text{des}} \end{bmatrix}^T, \quad (16)$$

where $K_J \in \mathbb{R}^n$ is the joint stiffness vector, which collects k_i in order, and $P_{i,\text{des}}$ is the desired pressure vector of i-th segment:

$$K_J = \begin{bmatrix} k_1 & \cdots & k_i & \cdots & k_n \end{bmatrix}^T,$$
$$P_{i,\text{des}} = \begin{bmatrix} P_{i,1,\text{des}} & P_{i,2,\text{des}} & P_{i,3,\text{des}} & P_{i,\text{core,des}} \end{bmatrix}^T, \quad (17)$$

The dynamics of the soft manipulator system with air pressure dynamics can be formulated in the following state space form:

$$\dot{x} = \begin{bmatrix} \dot{q} \\ \ddot{q} \\ \dot{K}_J \\ \dot{P} \end{bmatrix} = \begin{bmatrix} \dot{q} \\ M(q)^{-1} \left(A(q) \cdot T \cdot W \cdot P - \left(\frac{r}{R}\right)^2 K_{core}(P) q - V(q,\dot{q}) - D(q)\dot{q} - G(q) - \left[1 - \left(\frac{r}{R}\right)^2\right] K^0 q \right) \\ \begin{bmatrix} \dot{k}_1 & \cdots & \dot{k}_i & \cdots & \dot{k}_n \end{bmatrix}^T \\ \begin{bmatrix} \dot{P}_{1,1} & \dot{P}_{1,2} & \dot{P}_{1,3} & \dot{P}_{1,\text{core}} & \cdots & \dot{P}_{i,j} & \dot{P}_{i,\text{core}} & \cdots & \dot{P}_{n,1} & \dot{P}_{n,2} & \dot{P}_{n,3} & \dot{P}_{n,\text{core}} \end{bmatrix}^T \end{bmatrix}, \quad (18)$$

where the individual element $\dot{k}_i$ in $\dot{K}_J$ is defined in (15) and $\dot{P}_{i,j}$ and $\dot{P}_{i,\text{core}}$ in $\dot{P}$ are defined in (8) and (11), respectively.

B. Control in the Configuration Space

An NMPC is proposed to track the trajectory in the configuration space q, as well as the stiffness trajectory K_J. The primary idea of the NMPC is to find an optimal pressure input P_{des} at the current sampling instant to minimize the cost function J considering predicted future states over some horizon T. Since the optimization process of NMPC is realized in discrete-time domain, the discrete-time state space transformation is needed, which can be obtained by using a Runge-Kutta method of 4th order with a small step size δt [28]:

$$x_{k+1} = f_{\text{RK4}}(x_k, u_k, \delta t). \tag{19}$$

For the NMPC problem formulation, an optimal control problem is constructed in a sequential quadratic program (SQP) based on a direct multiple shooting approach [29]. The program computes a set of optimal control inputs within a control horizon subject to various constraints, including system dynamics, initial conditions and actuation pressure input boundaries:

$$\begin{aligned}\min_{P_{\text{des}}(k:k+m-1)} \sum_{i=0}^{p-1} (&\|q(k+i|k) - q_{\text{des}}(k+i|k)\|^2_{Q_q} \\ &+ \|K_J(k+i|k) - K_{J,\text{des}}(k+i|k)\|^2_{Q_K} \\ &+ \|P_{\text{des}}(k+i|k) - P_{\text{des}}(k+i-1|k)\|^2_{R}) \\ &+ \|P_{\text{des}}(k+i|k)\|^2_{S}\,,\end{aligned}$$

$$\begin{aligned}\text{s.t.} \quad & x_{k+i+1} = f_{\text{RK4}}(x_{k+i}, u_{k+i}, \delta t), \quad x_0 = x_{\text{init}}, \\ P_{\min} \leqslant P_{i,j,\text{des}}(k+i) \leqslant P_{\max}, \quad & V_{\min} \leqslant P_{i,\text{core}}(k+i) \leqslant V_{\max}, \\ & 0 \leq i \leq p-1. \end{aligned} \tag{20}$$

In the cost function of Eq. (20), m is the length of control horizon, $P_{\text{des}}(k:k+m-1)$ is the optimal desired pressure input sequence within the control horizon, which is from time k to time $k+m-1$, p is the length of the predictive horizon, $q(k+i|k)$ is the predicted configuration, $q_{\text{des}}(k+i|k)$ is the desired trajectory, $K_J(k+i|k)$ is the predicted stiffness, $K_{J,\text{des}}(k+i|k)$ is the desired stiffness, and $P_{\text{des}}(k+i|k)$ is the pressure input, which are all at instant $k+i$, estimated at instant k. Q_q, Q_K, R and S are the positive-definite weighting matrices of the curvature position, the stiffness, the change in pressure input, and the magnitude of pressure input, respectively. Note that the cost function is designed not only to track the desired curvature position and the desired curvature stiffness trajectory, but also to maintain lower energy consumption and smaller input variation to prevent valve chattering [22]. In the constraints of Eq. (20), the input $u_{k+i} = P_{\text{des}}(k+i|k)$ and if $m \leq p$, $u_{k+j} = u_{k+m-1}$ for $m \leq j \leq p-1$. x_{init} is the initial state, $P_{\min}$ and $P_{\max}$ are the inflation pressure boundaries in the air chambers, $V_{\min}$ and $V_{\max}$ are the vacuum pressure boundaries in the particle core chamber respectively. Note that, although the optimal input sequence $P_{\text{des}}(k:k+m-1)$ is available, only the first desired pressure input $P_{\text{des}}(k|k)$ is applied on the system at the current instant k.

Fig. 3 presents the block scheme of the system framework. During the NMPC solving process, the current state $\mathbf{x}$, the desired curvature position q_{des}, and the desired stiffness $K_{J,\text{des}}$ will be fed into the controller. Afterwards, the desired pressure input generated from the NMPC will be sent to the full system dynamics, which consists of pressure actuation dynamics and soft manipulator dynamics. Finally, the full state feedback is fed into the NMPC and the pressure state will feed back to the low-level pressure controller.

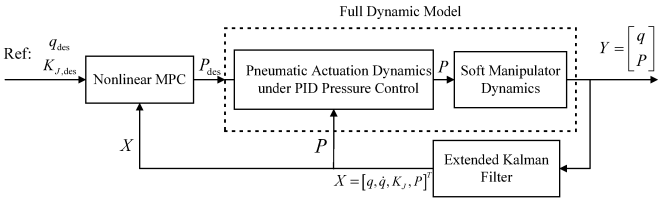

Fig. 3. Block scheme of the proposed nonlinear model predictive controller for the soft continuum manipulator with controllable stiffness. In this framework, the desired position trajectory in the configuration space and the stiffness trajectory are tracked at the same time.

Not all states in the system are measurable in real time. Specifically, there is no reliable sensor to measure the stiffness of the manipulator directly since the stiffness is typically calculated passively by experiment. Additionally, it is more accurate to detect the position of the manipulator via a motion capture system. Therefore, it is fair to assume the output of the full dynamic model as $[q, P]^T$. In order to obtain the full states, an extended Kalman filter (EKF) is utilized to estimate the velocity and stiffness states as shown in Fig. 3.

C. Control in the Task Space

To control the soft manipulator in the Cartesian coordinates, the previous control framework is extended to the task space. The conventional approach is to design an additional inverse kinematics branch to convert the desired task trajectory into the desired joint trajectory while other components remain the same. The common numerical inverse kinematics includes the Jacobian inverse kinematic method and the Jacobian transpose inverse kinematic method [30], but both of these require additional computation of the Jacobian matrix based on existing configuration space framework. Here we propose an extended framework exploiting the potential of the NMPC to implement a tracking task in the Cartesian coordinates.

The desired trajectory has been changed from the configuration space q_{des} to the task space e_{des}, which represents the coordinate vector of entire arm's end position. As shown in Fig. 4, a block of the forward kinematics based on Eq. (1) is added in the state feedback, computing the end position e in real time and feeding it into the NMPC. This extended NMPC controls the soft manipulator to minimize the Euclidean distance between the end point and the reference trajectory while maintaining tracking stiffness reference.

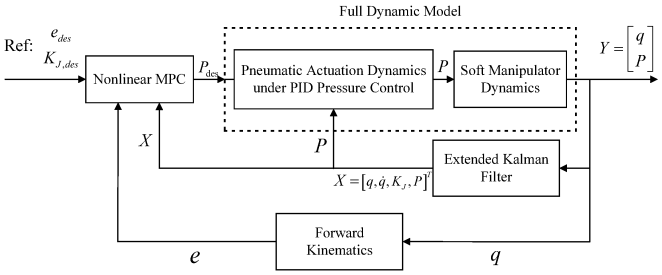

Fig. 4. Block scheme of the extended NMPC enabling the soft manipulator to track the desired position trajectory in the task space and the stiffness trajectory simultaneously.

The cost function of the NMPC in the task space is defined by replacing the configuration position error in Eq. (20) with the end position error in the task space:

$$\begin{aligned}\min_{P_{\text{des}}(k:k+m-1)} \sum_{i=0}^{p-1} \big(&\|e(k+i|k) - e_{\text{des}}(k+i|k)\|^2_{Q_e} \\ &+ \|K_J(k+i|k) - K_{J,\text{des}}(k+i|k)\|^2_{Q_K} \\ &+ \|P_{\text{des}}(k+i|k) - P_{\text{des}}(k+i-1|k)\|^2_{R}\big) \\ &+ \|P_{\text{des}}(k+i|k)\|^2_{S}\,, \end{aligned} \tag{21}$$

subject to the same constraints in Eq. (20).

IV. SIMULATION

In this section, the feasibility and effectiveness of the proposed NMPC framework in the configuration space and task space are validated in MATLAB simulation.

For simplicity, a soft continuum manipulator with a single segment is considered; multiple segments could be simulated in a similar fashion. The coefficient matrices M, V, G in dynamic equation Eq. (18) are obtained by using the Symbolic Math Toolbox and Euler-Lagrange Toolbox [31] in MATLAB. The robot parameters for simulation including the length $L_i = 0.11$ m, the mass $m_i = 0.15$ kg, the identified stiffness $k_i = 0.626$ Nm/(rad), and the identified damping $d_i = 0.029$ Nms/(rad) are taken from the reference [9]. The parameters in the full model Eq. (13) are taken as follows: actuator parameter $w = 8 \times 10^{-3}$ Nm/KPa, radius ratio $\frac{r}{R} = \frac{1}{2}$, coefficient $\alpha = 0.08$ Nm/(rad $\cdot$ KPa), and pneumatic dynamic parameters $a_0 = a_1 = b_0 = b_1 = 1$. Furthermore, the NMPC algorithm is implemented using the `fmincon` function with an SQP algorithm. A control horizon $m = 5$, and a predictive horizon $p = 10$ is used with input constrains $P_{\min} = 0$ KPa, $P_{\max} = 300$ kPa, $V_{\min} = 0$ KPa, and $V_{\max} = 100$ KPa. The system is run at 50 Hz.

For the configuration space, to test the control architecture in Section III B, the manipulator is controlled to track the desired configuration trajectory from an initial point $(\phi_1(0), \theta_1(0))^T = [3, 0.3]^T$ and to track the desired stiffness trajectory from an initial stiffness without particle jamming being active. A sinusoidal desired trajectory is selected,

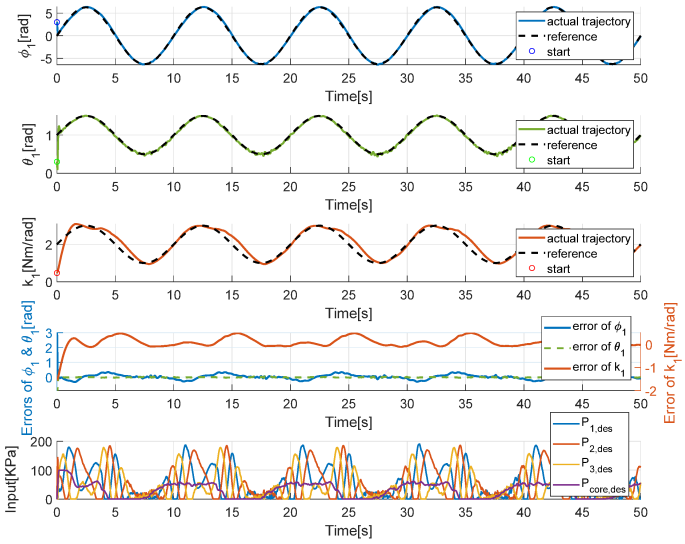

Fig. 5. Simulation results in the configuration space. The first three graphs demonstrate the trajectories of the actual configuration position ϕ_1 and θ_1 and the stiffness k_1 with the desired trajectory. The fourth graph shows the tracking error. The bottom graph shows the desired pressure control input.

TABLE I
WEIGHT PARAMETERS OF THE NMPC COST FUNCTION

Configuration Space		Task Space	
Weight	Value	Weight	Value
Q_q	diag$\{100, 300\}$	Q_e	diag$\{1000, 1000, 1000\}$
Q_K	3000	Q_K	2000
R	diag$\{2, 2, 2, 2\}$	R	diag$\{1, 1, 1, 1\}$
S	diag$\{0.08, 0.08, 0.08, 0.08\}$	S	diag$\{0.05, 0.05, 0.05, 0.05\}$

which is defined by the following function:

$$\begin{cases} \phi_{1,\text{des}}(t) = 2\pi \sin(\frac{\pi}{5}t) \\ \theta_{1,\text{des}}(t) = 0.5 \sin(\frac{\pi}{5}t) + 1 \\ k_{1,\text{des}}(t) = \sin(\frac{\pi}{5}t) + 2, \end{cases} \tag{22}$$

The weight parameters of the NMPC cost function in Eq. (20) are tuned to the values in Table I to achieve good tracking performance. Fig. 5 shows the performance of the NMPC framework in this case. The manipulator is able to track two configuration reference trajectories accurately, despite an added white noise with a magnitude of 0.01 rad and 1 KPa to the angle measurements and pressure measurements respectively. The desired stiffness trajectory is tracked with a small delay, but the error of tracking is relatively small compared to the amplitude of the reference trajectory. As shown in Fig. 5, all desired pressure inputs do not exceed their constraints and vary smoothly.

Furthermore, the performance of the NMPC framework is tested in the task space by controlling the end position of the manipulator to track the desired trajectory in the Cartesian coordinates. The initial point is $(\phi_1(0), \theta_1(0))^T = [1, 0.1]^T$ and a circular reference trajectory with the same height is

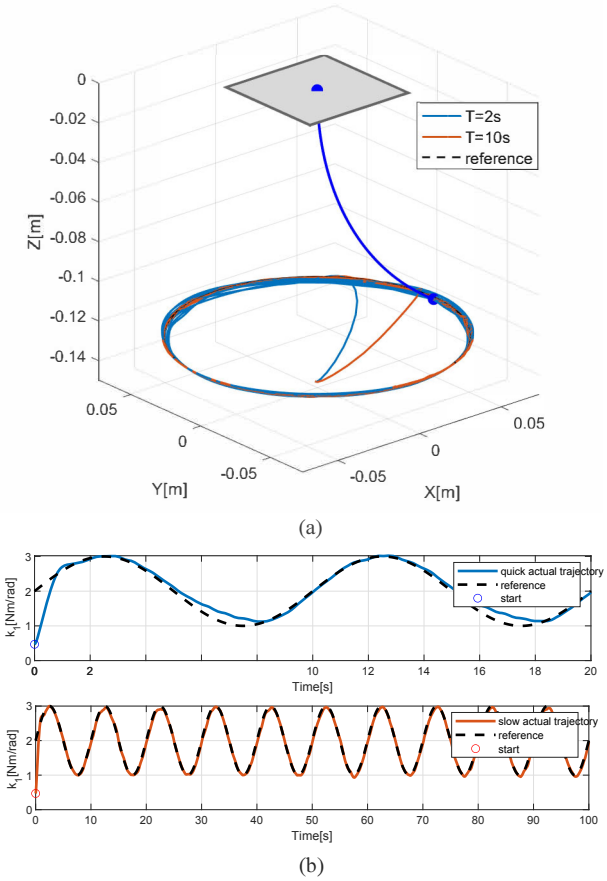

Fig. 6. Simulation results in the task space. Panel (a) shows the desired trajectory and actual trajectory in 3D space with two different periods of 2s and 10s respectively. Panel (b) shows the performance of tracking the desired stiffness trajectory in the faster and slower cases respectively.

defined as:

$$e_{\text{des}}(t) = \begin{bmatrix} 0.0716\cos(\varpi t) & 0.0716\sin(\varpi t) & -0.124 \end{bmatrix}^T, \tag{23}$$

where ϖ is a constant used to tune the velocity of the reference trajectory. The desired stiffness trajectory is the same as the one in Eq. (22). In order to test the versatility of the proposed controller under different desired speeds, the system is tested with $\varpi = \pi$ and $\varpi = 0.2\pi$, making the periods of the references 2s and 10s. The weight parameters used in the NMPC cost function from Eq. (21) are listed in Table I. To validate the robustness of the controller, white noises with magnitudes of 0.01 m and 1 KPa are added to the measurements of $[q, P]^T$. In order to compare the performance with different velocities clearly, the simulation durations are set to 20s and 100s for $\varpi = \pi$ and $\varpi = 0.2\pi$ respectively, guaranteeing tracking the circle ten times. The tracking performance of these two trajectories is shown in Fig. 6. The end position of the manipulator is approaching the desired circular trajectory in the task space and the desired stiffness trajectory simultaneously with minimal overshooting and oscillations. Based on the position data outside of the first unstable period, the average and maximum Euclidean distance error for tracking the quick and slow

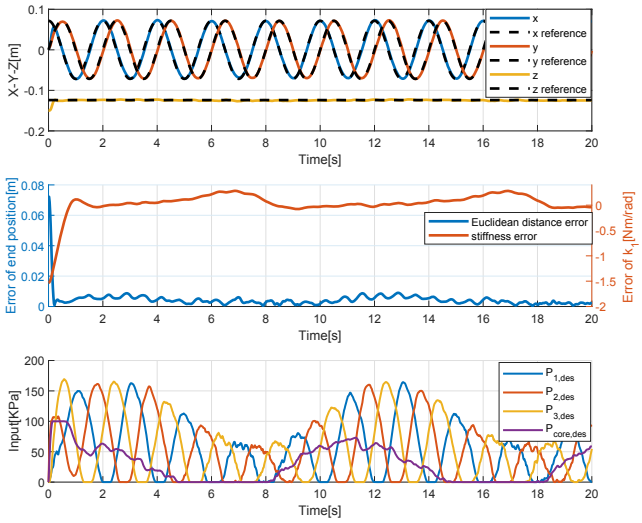

Fig. 7. The performance of the tracking error and the desired pressure control input when tracking the quick reference ($\varpi = \pi$).

TABLE II
AVERAGE AND MAXIMUM EUCLIDEAN DISTANCE ERROR OF TRACKING THE SLOW AND QUICK REFERENCES IN THE TASK SPACE

	Avg. Euclidean distance error(m)	Max. Euclidean distance error(m)
Slow reference($\varpi = 0.2\pi$)	0.001	0.0052
Quick reference($\varpi = \pi$)	0.0039	0.0090

references are computed as shown in Table II. As expected, the tracking error of the faster reference is greater than that of the slower one. However, it can be seen that the NMPC framework still works with a high velocity, considering that the error is negligible compared to the length of manipulator and the size of workspace. Only the results from tracking the faster reference are shown in Fig. 7 since those from the slower reference show a similar, but less siginificant error. Indeed, the faster position reference, as well as the stiffness reference, are tracked accurately by the manipulator. The performance of the slower trajectory is predicted to be better than that of the faster trajectory according to the results shown in Table II.

V. CONCLUSION

In this work, we constructed a dynamic model with tunable stiffness for soft continuum manipulators and proposed an NMPC in the configuration space as well as in the task space. The NMPC architecture was firstly aimed at tracking a desired configuration trajectory as well as a desired stiffness trajectory. The stiffness and velocity of the manipulator are estimated using an extended Kalman filter. The controller enables the manipulator to track a desired task-space trajectory as well as a desired stiffness trajectory. Furthermore, the feasibility and robustness of the controller have been validated through simulation.

Future research will focus on advancing the modeling and computation techniques. For example, the length of the

manipulator could be integrated into the model since the inflation pressure leads to elongations. Recent research has considered this phenomenon by adjusting the selection of configuration parameters [32], [33]. Additionally, the relationship between the segment stiffness and Cartesian stiffness is also worthwhile to explore. The control strategy based on NMPC requires high computation, and faster approaches such as adaptive linear MPC can be investigated in the future. Finally, experiments will be conducted on soft pneumatic manipulators with tunable stiffness to validate the proposed control approaches.

ACKNOWLEDGMENT

We gratefully acknowledge Demetris Coleman for his assistance on nonlinear MPC programming.

REFERENCES

[1] S. Chen, Y. Pang, Y. Cao, X. Tan, and C. Cao, "Soft robotic manipulation system capable of stiffness variation and dexterous operation for safe human–machine interactions," *Advanced Materials Technologies*, vol. 6, no. 5, p. 2100084, 2021.

[2] P. Polygerinos, S. Lyne, Z. Wang, L. F. Nicolini, B. Mosadegh, G. M. Whitesides, and C. J. Walsh, "Towards a soft pneumatic glove for hand rehabilitation," in *2013 IEEE/RSJ International Conference on Intelligent Robots and Systems*. IEEE, 2013, pp. 1512–1517.

[3] M. Cianchetti, T. Ranzani, G. Gerboni, I. De Falco, C. Laschi, and A. Menciassi, "Stiff-flop surgical manipulator: Mechanical design and experimental characterization of the single module," in *2013 IEEE/RSJ International Conference on Intelligent Robots and Systems*. IEEE, 2013, pp. 3576–3581.

[4] X. Chen, X. Zhang, Y. Huang, L. Cao, and J. Liu, "A review of soft manipulator research, applications, and opportunities," *Journal of Field Robotics*, vol. 39, no. 3, pp. 281–311, 2022.

[5] X. You, Y. Zhang, X. Chen, X. Liu, Z. Wang, H. Jiang, and X. Chen, "Model-free control for soft manipulators based on reinforcement learning," in *2017 IEEE/RSJ International Conference on Intelligent Robots and Systems (IROS)*. IEEE, 2017, pp. 2909–2915.

[6] K.-H. Lee, D. K. Fu, M. C. Leong, M. Chow, H.-C. Fu, K. Althoefer, K. Y. Sze, C.-K. Yeung, and K.-W. Kwok, "Nonparametric online learning control for soft continuum robot: An enabling technique for effective endoscopic navigation," *Soft Robotics*, vol. 4, no. 4, pp. 324–337, 2017.

[7] W. S. Rone and P. Ben-Tzvi, "Continuum robot dynamics utilizing the principle of virtual power," *IEEE Transactions on Robotics*, vol. 30, no. 1, pp. 275–287, 2013.

[8] H. Wang, C. Wang, W. Chen, X. Liang, and Y. Liu, "Three-dimensional dynamics for cable-driven soft manipulator," *IEEE/ASME Transactions on Mechatronics*, vol. 22, no. 1, pp. 18–28, 2016.

[9] R. K. Katzschmann, C. Della Santina, Y. Toshimitsu, A. Bicchi, and D. Rus, "Dynamic motion control of multi-segment soft robots using piecewise constant curvature matched with an augmented rigid body model," in *2019 2nd IEEE International Conference on Soft Robotics (RoboSoft)*. IEEE, 2019, pp. 454–461.

[10] M. Trumić, C. Della Santina, K. Jovanović, and A. Fagiolini, "Adaptive control of soft robots based on an enhanced 3D augmented rigid robot matching," in *2021 American Control Conference (ACC)*. IEEE, 2021, pp. 4991–4996.

[11] F. A. Spinelli and R. K. Katzschmann, "A unified and modular model predictive control framework for soft continuum manipulators under internal and external constraints," *arXiv preprint arXiv:2204.13710*, 2022.

[12] A. Kazemipour, O. Fischer, Y. Toshimitsu, K. W. Wong, and R. K. Katzschmann, "Adaptive dynamic sliding mode control of soft continuum manipulators," in *2022 International Conference on Robotics and Automation (ICRA)*. IEEE, 2022, pp. 3259–3265.

[13] M. Al-Rubaiai, T. Pinto, C. Qian, and X. Tan, "Soft actuators with stiffness and shape modulation using 3D-printed conductive polylactic acid material," *Soft Robotics*, vol. 6, no. 3, pp. 318–332, 2019.

[14] Y. Ansari, M. Manti, E. Falotico, M. Cianchetti, and C. Laschi, "Multiobjective optimization for stiffness and position control in a soft robot arm module," *IEEE Robotics and Automation Letters*, vol. 3, no. 1, pp. 108–115, 2017.

[15] P. Jiang, Y. Yang, M. Z. Chen, and Y. Chen, "A variable stiffness gripper based on differential drive particle jamming," *Bioinspiration & Biomimetics*, vol. 14, no. 3, p. 036009, 2019.

[16] Y. Yang, Y. Zhang, Z. Kan, J. Zeng, and M. Y. Wang, "Hybrid jamming for bioinspired soft robotic fingers," *Soft Robotics*, vol. 7, no. 3, pp. 292–308, 2020.

[17] S. Wolf, G. Grioli, O. Eiberger, W. Friedl, M. Grebenstein, H. Höppner, E. Burdet, D. G. Caldwell, R. Carloni, M. G. Catalano, L. Dirk, S. Stefano, T. Nikos, D. Michaël Van, H. Ronald Van, V. Bram, V. Ludo C., B. Antonio, and A. Albu-Schäffer, "Variable stiffness actuators: Review on design and components," *IEEE/ASME Transactions on Mechatronics*, vol. 21, no. 5, pp. 2418–2430, 2015.

[18] C. M. Best, L. Rupert, and M. D. Killpack, "Comparing model-based control methods for simultaneous stiffness and position control of inflatable soft robots," *The International Journal of Robotics Research*, vol. 40, no. 1, pp. 470–493, 2021.

[19] P. Polygerinos, Z. Wang, K. C. Galloway, R. J. Wood, and C. J. Walsh, "Soft robotic glove for combined assistance and at-home rehabilitation," *Robotics and Autonomous Systems*, vol. 73, pp. 135–143, 2015.

[20] R. J. Webster III and B. A. Jones, "Design and kinematic modeling of constant curvature continuum robots: A review," *The International Journal of Robotics Research*, vol. 29, no. 13, pp. 1661–1683, 2010.

[21] V. Falkenhahn, T. Mahl, A. Hildebrandt, R. Neumann, and O. Sawodny, "Dynamic modeling of constant curvature continuum robots using the Euler-Lagrange formalism," in *2014 IEEE/RSJ international conference on intelligent robots and systems*. IEEE, 2014, pp. 2428–2433.

[22] M. T. Gillespie, C. M. Best, and M. D. Killpack, "Simultaneous position and stiffness control for an inflatable soft robot," in *2016 IEEE International Conference on Robotics and Automation (ICRA)*. IEEE, 2016, pp. 1095–1101.

[23] S. G. Fitzgerald, G. W. Delaney, and D. Howard, "A review of jamming actuation in soft robotics," in *Actuators*, vol. 9, no. 4. MDPI, 2020, p. 104.

[24] M. Manti, V. Cacucciolo, and M. Cianchetti, "Stiffening in soft robotics: A review of the state of the art," *IEEE Robotics & Automation Magazine*, vol. 23, no. 3, pp. 93–106, 2016.

[25] N. G. Cheng, M. B. Lobovsky, S. J. Keating, A. M. Setapen, K. I. Gero, A. E. Hosoi, and K. D. Iagnemma, "Design and analysis of a robust, low-cost, highly articulated manipulator enabled by jamming of granular media," in *2012 IEEE International Conference on Robotics and Automation*. IEEE, 2012, pp. 4328–4333.

[26] Y. Li, Y. Chen, Y. Yang, and Y. Wei, "Passive particle jamming and its stiffening of soft robotic grippers," *IEEE Transactions on Robotics*, vol. 33, no. 2, pp. 446–455, 2017.

[27] C. Della Santina, R. K. Katzschmann, A. Bicchi, and D. Rus, "Model-based dynamic feedback control of a planar soft robot: Trajectory tracking and interaction with the environment," *The International Journal of Robotics Research*, vol. 39, no. 4, pp. 490–513, 2020.

[28] D. Hanover, P. Foehn, S. Sun, E. Kaufmann, and D. Scaramuzza, "Performance, precision, and payloads: Adaptive nonlinear MPC for quadrotors," *IEEE Robotics and Automation Letters*, vol. 7, no. 2, pp. 690–697, 2021.

[29] T. A. Johansen, "Introduction to nonlinear model predictive control and moving horizon estimation," *Selected topics on Constrained and Nonlinear Control*, vol. 1, pp. 1–53, 2011.

[30] M. W. Spong, S. Hutchinson, and M. Vidyasagar, *Robot Modeling and Control*. John Wiley & Sons, 2020.

[31] M. Kim, "Euler lagrange tool package," Oct. 2016. [Online]. Available: https://www.mathworks.com/matlabcentral/fileexchange/49796-euler-lagrange-tool-package

[32] C. Della Santina, A. Bicchi, and D. Rus, "On an improved state parametrization for soft robots with piecewise constant curvature and its use in model based control," *IEEE Robotics and Automation Letters*, vol. 5, no. 2, pp. 1001–1008, 2020.

[33] Y. Toshimitsu, K. W. Wong, T. Buchner, and R. Katzschmann, "SoPrA: Fabrication & dynamical modeling of a scalable soft continuum robotic arm with integrated proprioceptive sensing," in *2021 IEEE/RSJ International Conference on Intelligent Robots and Systems (IROS)*. IEEE, 2021, pp. 653–660.